Design and Performance of the Monopulse Control System

W. Gawronski[1] and M. A. Gudim[1]

Ka-band (32-GHz) monopulse tracking has been chosen for the upcoming NASA missions. This decision requires an increased pointing accuracy of the Deep Space Network antenna servo systems that are maintained in a noisy environment. The noise sources include wind gusts, encoder imperfections, and Block V Receiver (BVR) noise. This article describes the selection of the position and monopulse controllers for the improved tracking accuracy and presents the results of the linear and nonlinear simulations to confirm that servo performance meets the requirements.

I. Introduction

The requirement of a 1.54-mdeg mean radial pointing error (1.23-mdeg rms error in elevation and cross-elevation) imposes new demands on the properties of the beam-waveguide (BWG) antenna position servo. The servo should have an expanded bandwidth of 1 Hz and improved disturbance rejection properties. This is achieved with the implementation of the high-gain linear, quadratic, Gaussian (LQG) controllers (linear system, quadratic performance index, Gaussian-noise), as reported in [1]. This article presents the selection of the monopulse controller and analyzes the monopulse tracking errors in a noisy environment. In the simulations, we made an effort to reflect as closely as possible the real antenna environment. For example, the antenna model was derived from the field test data using the system identification procedure; encoder error disturbances, servo noise, and wind gusts were obtained from the field data; and Block V Receiver (BVR) noise was obtained as a tracking-loop jitter derived from the phase-locked loop equations.

II. Selecting the Monopulse Controller

In this section, the monopulse controller is selected, and the properties of the monopulse closed-loop system are evaluated. The monopulse feedback loop is closed over the antenna position loop (see the block diagram in Fig. 1 for the elevation-axis controller). The monopulse control system consists of the antenna position loop model, the monopulse controller, and the monopulse receiver. The latter consists of the feed, the low-noise amplifier, and the BVR. Two monopulse control systems are designed and evaluated: the first one with the proportional and integral (PI) controller in the position loop and the second one with the LQG controller in the position loop.

[1] Communications Ground Systems Section.

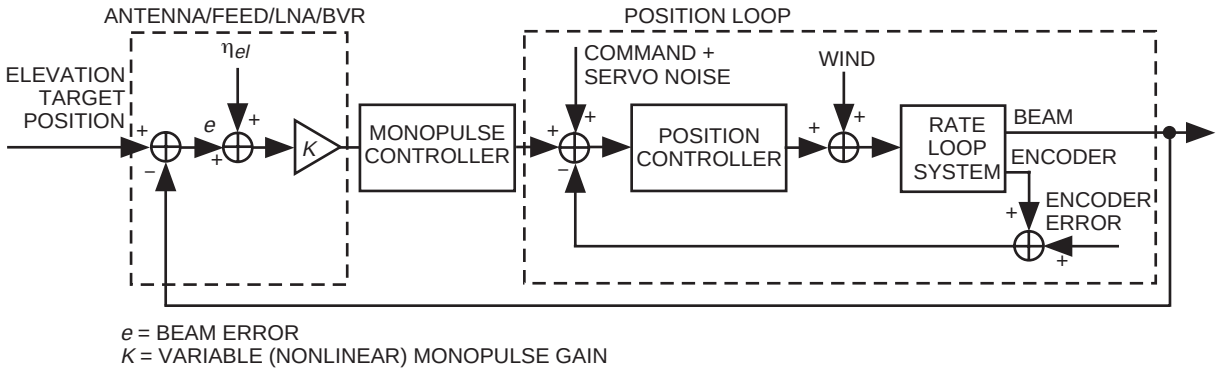

Fig. 1. Block diagram of the monopulse control system, elevation axis.

In the design process, the following conditions were assumed:

(1) Azimuth and control loops are independent. This was confirmed analytically and in the field (see [2] and [1]).

(2) The antenna elevation position is 10 deg; thus, the azimuth and the cross-elevation errors are approximately the same.

(3) The receiver sensitivity function, γ, is constant; that is, $\gamma(\theta, \varphi) = 70.6$ V/V/deg, where θ and φ are the magnitude and phase of the pointing error.

(4) Noises in elevation and cross-elevation channels are independent.

The properties of the monopulse loop depend on the properties of the position loop. The magnitudes and phases of the position-loop transfer functions are shown in Figs. 2 and 3 (solid lines). In order to meet the tracking requirements, the position loop was designed such that its transfer function for low frequencies (up to the frequency denoted f_o) is approximately equal to 1. The frequency f_o is called a bandwidth, and for the PI controller, $f_o = 0.1$ Hz, and for the LQG controller, $f_o = 1.0$ Hz. For frequencies higher than f_o, the position-loop transfer function rolls off, although it contains resonance

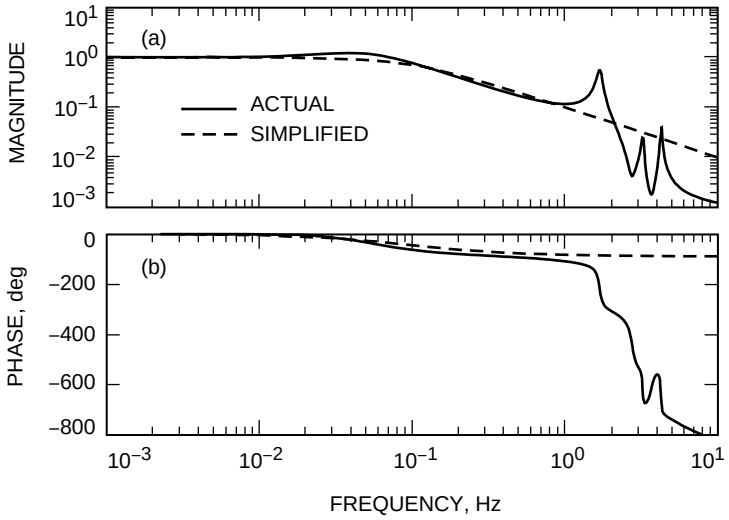

Fig. 2. The transfer function of the PI position control loop: (a) magnitude and (b) phase.

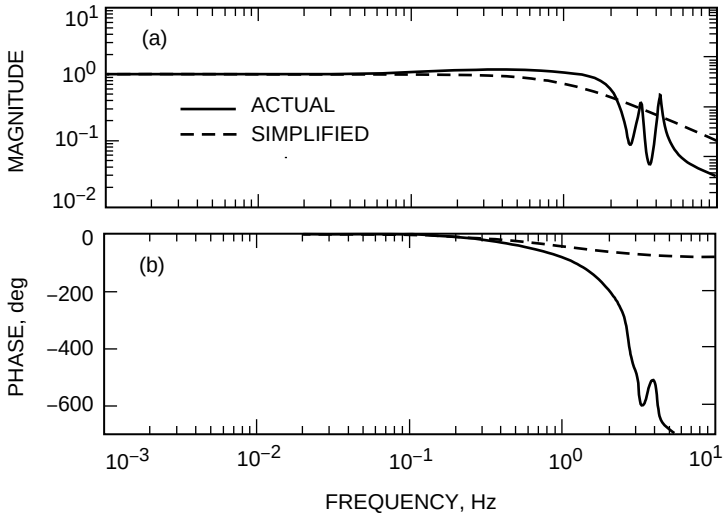

Fig. 3. The transfer function of the LQG position control loop: (a) magnitude and (b) phase.

peaks that reflect the antenna flexible deformations. For monopulse design purposes, the peaks are ignored, and the high-frequency part of the position-loop transfer function can be approximated with the slope of −20 dB/dec. Therefore, for monopulse design purposes, the position loop is approximated with the first-order transfer function

$$G(s) = \frac{1}{1+Ts} \tag{1}$$

It has a unit gain and the time constant reciprocal to the bandwidth, $T = 1/(2\pi f_o)$. The time constant is different for the PI and LQG controllers, namely, $T = 1.592$ s for the PI system and $T = 0.159$ s for the LQG system. The magnitudes and phases of the transfer functions of the simplified models are shown in Figs. 2 and 3 (dashed lines).

Based on the above model, the controller is designed. It includes the determination of its transfer function and the tracking and disturbance rejection properties.

A. Selecting the Transfer Function of the Monopulse Controller

In this subsection, the transfer function $F(s)$ of the monopulse controller is determined. The block diagram of the simplified monopulse control system is presented in Fig. 4. In this diagram, α denotes the target location, y is the beam position, e is beam error, and r is the command (or predict). Denote the transfer functions from α to y by H, those from r to y by H_r, and the transfer function of the position loop by G. From Fig. 4, we obtain

$$\left.\begin{aligned} H(s) &= \frac{y(s)}{\alpha(s)} = \frac{GF}{1+GF} \\ H_r(s) &= \frac{y(s)}{r(s)} = \frac{G}{1+GF} \end{aligned}\right\} \tag{2}$$

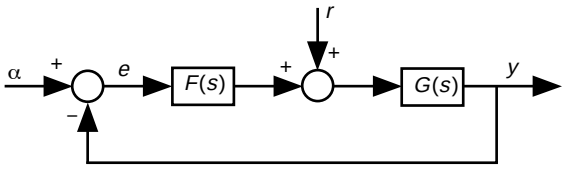

Fig. 4. A simplified block diagram of the monopulse control system.

Using the plant transfer function $G(s)$ as in Eq. (1), we arrive at

$$\left.\begin{aligned} H(s) &= \frac{F(s)}{1+Ts+F(s)} \\ H_r(s) &= \frac{1}{1+Ts+F(s)} \end{aligned}\right\} \tag{3}$$

The controller transfer function $F(s)$ is determined by shaping the tracking properties of the monopulse system, $H(s)$. For good tracking properties, it is required that the magnitude of the transfer function within the bandwidth $0 \le \omega \le 1/T$ be equal to 1, i.e.,

$$|H(\omega)| = 1, \quad 0 \le \omega \le \frac{1}{T} \tag{4a}$$

From Eq. (3), it follows that the above condition is satisfied for

$$|F| >> 1, \quad 0 \le \omega \le \frac{1}{T} \tag{4b}$$

On the other hand, outside the bandwidth, for $\omega > 1/T$ it is required that

$$|H| \to 0, \quad \omega > \frac{1}{T} \tag{5a}$$

From Eq. (3), it follows that the above condition is satisfied for

$$|F| \to 0, \quad \omega > \frac{1}{T} \tag{5b}$$

Finally, for a reasonable stability margin, the roll-off rate of F at the crossover frequency should be 20 dB/dec (see [3, p. 25]).

It is easy to see that the transfer function of an integrator

$$F(s) = \frac{k}{s} \tag{6}$$

satisfies all of the above conditions. Thus, an integrator is chosen as a monopulse controller. Its gain, k, was chosen to obtain acceptable tracking properties. Namely, $k = 0.75$ was determined for the PI position-loop system and $k = 1.0$ for the LQG position-loop system. The selection was backed with extensive simulations of the tracking properties of the closed-loop system.

B. Comparison of the Simplified and Full-Order Monopulse Control Systems

Introducing Eq. (6) to Eq. (2), one obtains the closed-loop transfer function $H(s)$ of the second order:

$$H(s) = \frac{\omega_o^2}{s^2 + 2\zeta\omega_o s + \omega_o^2} \tag{7}$$

where $\omega_o = \sqrt{k/T}$ and $\zeta = 1/(2\sqrt{kT})$. The monopulse closed-loop parameters are compared in Table 1.

Table 1. Monopulse closed-loop parameters.

Controller	T, s	k, s^{-1}	ω_o, rad/s	f_o, Hz	ζ
PI	1.592	0.75	0.69	0.11	0.46
LQG	0.159	1.0	2.51	0.40	1.25

The plots of the simplified (dashed line) and full-order (solid line) transfer functions of the monopulse closed-loop system are shown in Fig. 5 (with the PI position controller) and Fig. 6 (with the LQG position controller), showing satisfactory coincidence. Note that the monopulse system with the PI controller is narrowbanded ($f_o = 0.11$ Hz) and underdamped (the damping ratio is smaller than the critical one, $\zeta = 0.46 < \zeta_{\text{critical}}$, where $\zeta_{\text{critical}} = 0.71$), while the bandwidth of the monopulse system with the LQG controller is wider ($f_o = 0.40$ Hz) and overdamped (the damping ratio is larger than the critical one, $\zeta = 1.25 > \zeta_{\text{critical}}$). Thus, the monopulse system with the PI position loop exhibits overshoot and longer settling time in the step response, while the monopulse system with the LQG position loop has no overshoot and a shorter settling time.

Within the bandwidth, the simplified and the full-order system show good coincidence in terms of the properties used in the controller design and stability analysis. However, only the full-order system can give reliable error estimates of the pointing errors with the required precision.

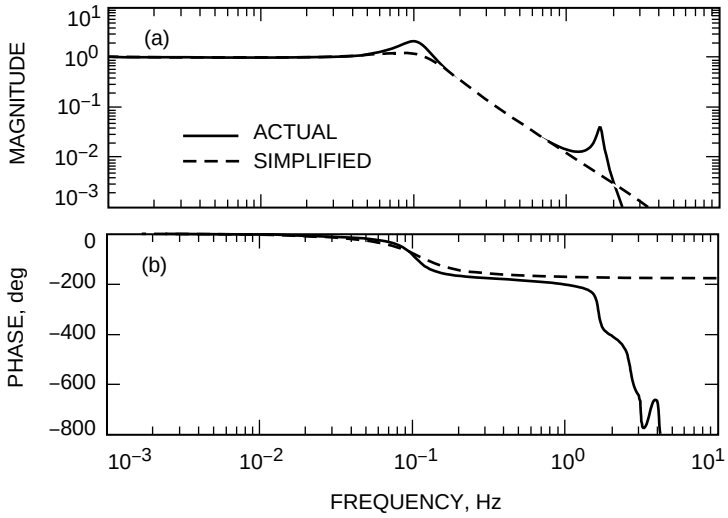

Fig. 5. The transfer function of the monopulse control system with the PI position control loop: (a) magnitude and (b) phase.

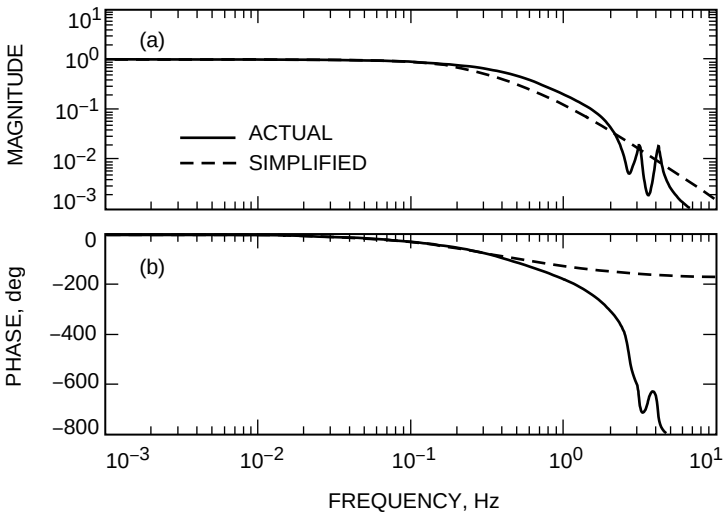

Fig. 6. The transfer function of the monopulse control system with the LQG position control loop: (a) magnitude and (b) phase.

C. Disturbance-Rejection Properties

Note first that the transfer function $H_r(s)$ from the command to the encoder also is the transfer function from the encoder disturbances to the encoder. It describes the system disturbance rejection properties and can be obtained by introducing Eq. (6) to the second transfer function in Eq. (3):

$$H_r(s) = \frac{2\zeta\omega_o s}{s^2 + 2\zeta\omega_o s + \omega_o^2} \tag{8}$$

The plots of this transfer function (dashed line) and of the full-order transfer function (solid line) for the system with the PI controller are compared in Fig.7 and in Fig. 8 for the system with the LQG controller.

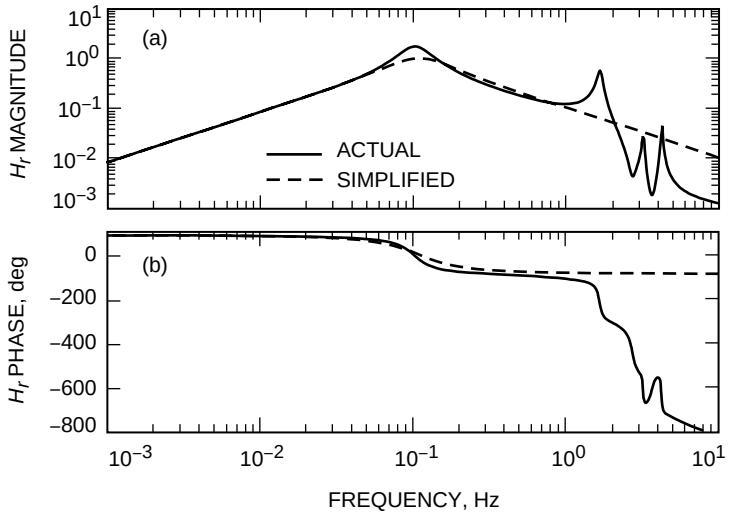

Fig. 7. The disturbance transfer function of the monopulse control system with the PI position control loop: (a) magnitude and (b) phase.

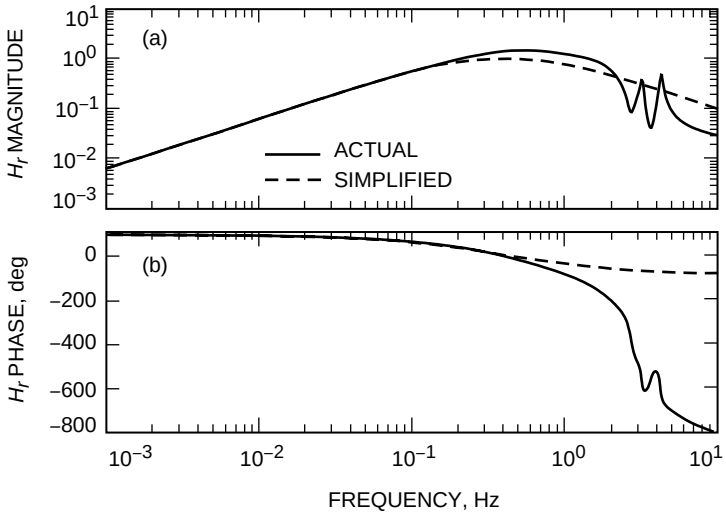

Fig. 8. The disturbance transfer function of the monopulse control system with the LQG position control loop: (a) magnitude and (b) phase.

These figures show good coincidence within the bandwidth and justify the use of a simplified model for design purposes. They also show that the low- and the high-frequency disturbances are significantly suppressed. However, there is a frequency interval, around 0.1 Hz for the PI system and around 1 Hz for the LQG system, in which the disturbance rejection is not as effective.

The disturbance rejection properties of the PI and LQG system are compared in Fig. 9. In low frequencies up to 0.2 Hz, the LQG system is more effective than is the PI system. For higher frequencies, the PI system is more effective, acting as a low-pass filter.

The simplified model of the position-loop system does not include the wind disturbances. These disturbances will be presented with the full-position model only. The plots of the transfer function from the wind gusts input to the encoder output are given in Fig. 10: the solid line for the PI position loop and the dashed line for the LQG position loop. It is easy to see that the monopulse system with the LQG position loop has wind-disturbance rejection properties of an order of magnitude better than has the monopulse system with the PI position loop. This will be illustrated later with the results of the wind gusts simulations.

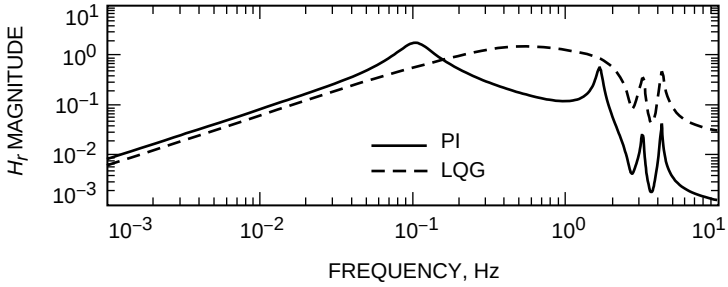

Fig. 9. A comparison of the disturbance transfer functions of the monopulse control systems with the PI position control loop and the LQG position control loop.

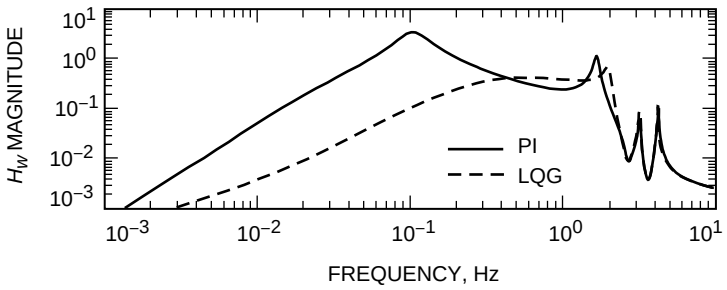

Fig. 10. A comparison of the wind transfer functions of the monopulse control systems with the PI position control loop and the LQG position control loop.

D. Stability Due to the Gain Variation

The monopulse gain, k, is slowly but significantly varying. Therefore, it is important to check the maximal gain for which the system is stable. The critical gains for which the system is still stable were obtained from simulations and are given in Table 2. For the PI position loop, the critical gains are 8.3 in azimuth and 16.7 in elevation. Since the nominal value of the gain for the PI controller is $k = 0.75$, the stability margin is large enough. For the LQG position loop, the critical gains are 5.9 in azimuth and 7.1 in elevation. Since the nominal value of the gain for the LQG controller is $k = 1.0$, this is also an acceptable stability margin. However, one has to notice that the LQG controller is the model-based one and that the rate-loop model varies slightly with the antenna elevation angle. These variations mainly impact the azimuth loop, and the stability margins for this loop could be slightly lower than those obtained from the simulations.

The performance under the varied gain is discussed in the next section.

Table 2. Critical gains.

Axis	PI	LQG
Azimuth	8.3	5.9
Elevation	16.7	7.1

III. Performance Simulations: Linear Model

The full-order model of the antenna, obtained from the field tests and the system identification, is used for the monopulse closed-loop performance evaluation. The following disturbances were used in the simulations:

(1) The 25 km/h wind gusts. The wind-disturbance model was taken from the field-measured data (see [4]). Typically, wind disturbances of 25 km/h in the PI position-loop system cause a 0.18-mdeg azimuth encoder error and a 2.0-mdeg elevation encoder error (standard deviation).

(2) The servo noise, generated by the white-noise input. This noise generates encoder jitters of about 0.1-mdeg standard deviation.[2]

[2] Observations by L. Alvarez, Communications Ground Systems Section, Jet Propulsion Laboratory, Pasadena, California.

(3) The azimuth encoder errors[3] (see Fig. 11, solid line). It consists of the radial run-out error, jitters, and rapid changes due to the gaps between the encoder segments.

(4) The BVR noise. It is a white noise of 1-mdeg standard deviation.[4]

The performance of the monopulse closed-loop system is characterized by the step response settling time and overshoot and by the transfer function bandwidth. The step responses for the nominal gains are given in Fig. 12; the transfer functions were presented earlier in Figs. 5 and 6. Settling time, overshoot, and bandwidth are summarized in Figs.13(a), 13(b), and 13(c) (azimuth) and in Figs. 13(d), 13 (e), and 13 (f) (elevation) for the nominal gain (1), for the reduced gain (0.5 of the nominal one), and for increased gains (2 and 4 times the nominal gain). The LQG controller has wider bandwidth, smaller settling time, and smaller overshoot as compared with the PI-controller performance.

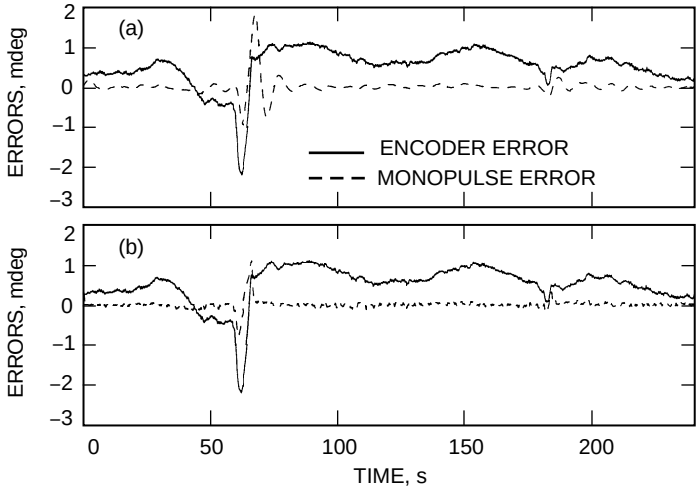

Fig. 11. Encoder and monopulse errors of the: (a) PI control system and (b) LQG control system.

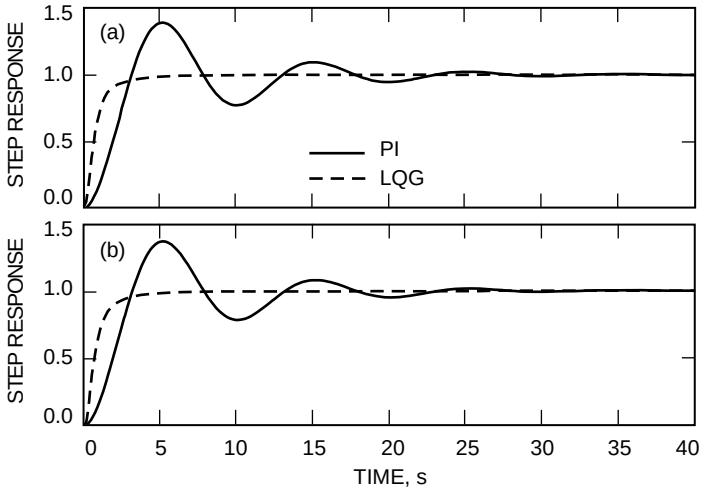

Fig. 12. Step responses of the PI and LQG monopulse systems: (a) azimuth and (b) elevation.

[3] As measured and reported by D. Strain, Communications Ground Systems Section, Jet Propulsion Laboratory, Pasadena, California.

[4] As reported by M. Gudim, Communications Ground Systems Section, Jet Propulsion Laboratory, Pasadena, California.

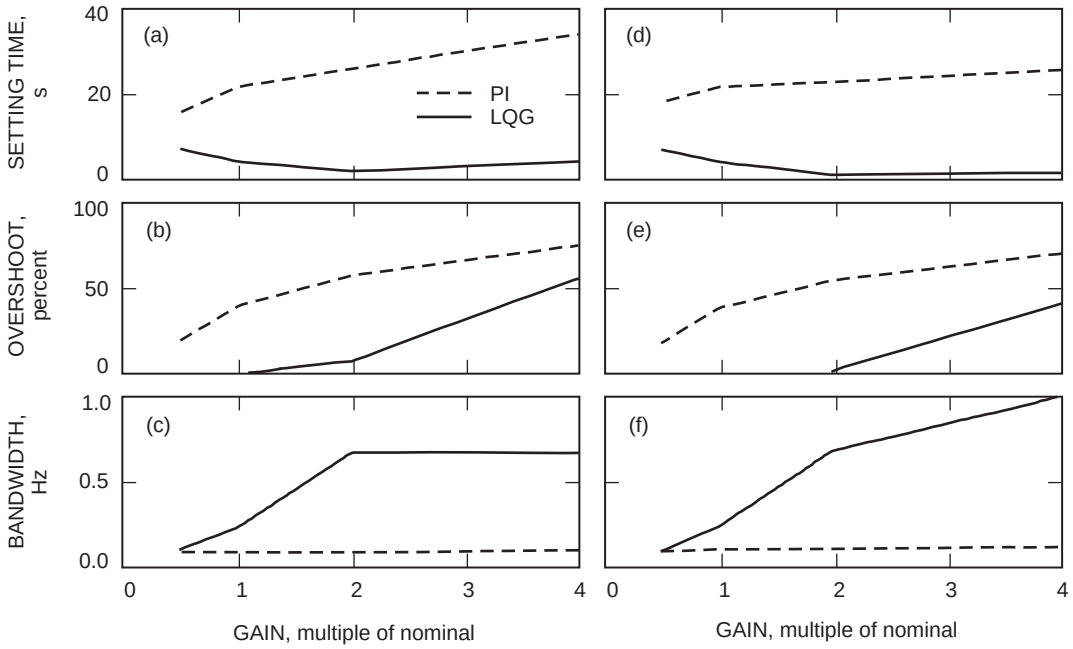

Fig. 13. Monopulse system performance for varied gains: (a) azimuth settling time, (b) azimuth overshoot, (c) azimuth bandwidth, (d) elevation settling time, (e) elevation overshoot, and (f) elevation bandwidth.

The results of pointing simulations due to each of the above-mentioned disturbances are given in Fig. 14, and the total errors are provided in Fig. 15 (solid line for the LQG and dashed line for the PI). They are obtained for the nominal monopulse gains ($k = k_{nom}$, where $k_{nom} = 0.75$ for the PI controller and $k_{nom} = 1.0$ for the LQG controller). The simulations also were performed for the varying gain, $k = \alpha k_{nom}$, i.e. for the reduced gain ($\alpha = 0.5$) and for increased gains ($\alpha = 2$ and $\alpha = 4$). The figures show that the elevation monopulse system with the PI controller does not meet the requirements, since the total error is 1.23 mdeg for the nominal gain. The bulk of this error is due to wind gusts. However, the LQG controller suppresses the wind disturbances enough to meet the requirements (see Figs. 14 and 15).

IV. Performance Simulations: Nonlinear Model

The monopulse pointing-error model combines the antenna, feed, low-noise amplifier, and BVR. This model is a nonlinear one, and the elevation and cross-elevation errors are not independent. The nonlinear monopulse pointing-error detector is incorporated into the control system model. The combined control system model that includes both axes and the nonlinear monopulse model is shown in Figs. 16(a) and 16 (b). It consists of the antenna rate loop model, the position controller, the monopulse controller with variable gain k, the monopulse sum $g(\theta, \phi)$ and difference $h(\theta, \phi)$ functions, the BVR monopulse processing block, and the conversion block of elevation and cross-elevation errors into elevation and azimuth errors (θ and φ are the magnitude and phase of the error, respectively). This model includes the following signals: encoder errors, commands, servo noise, wind disturbances, and main and error signal noises. The finite null depth of the detector function was modeled by adding a coherent signal to the difference pattern $h(\theta, \phi)$. The imbalance between the main and the error channels was modeled by adding phase error $\Delta\phi_{calib}$. BVR noises (noises in error detection), η_{el} and η_{xel}, and the receiver demodulation noise, η_{ϕ_c}, were added to the BVR monopulse processing block.

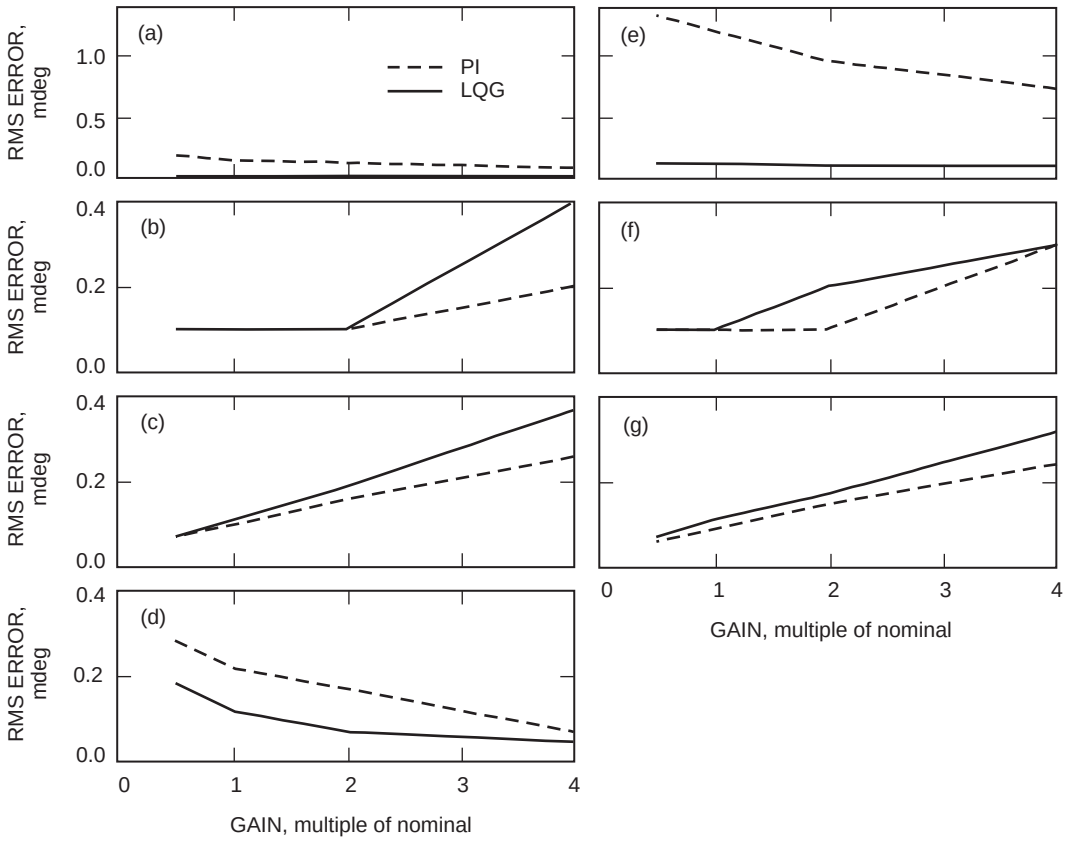

Fig. 14. Monopulse system errors under various disturbances: (a) azimuth 25-km/h wind, (b) azimuth servo noise, (c) azimuth BVR noise, (d) azimuth encoder error, (e) elevation 25-km/h wind, (f) elevation servo noise, and (g) elevation BVR noise.

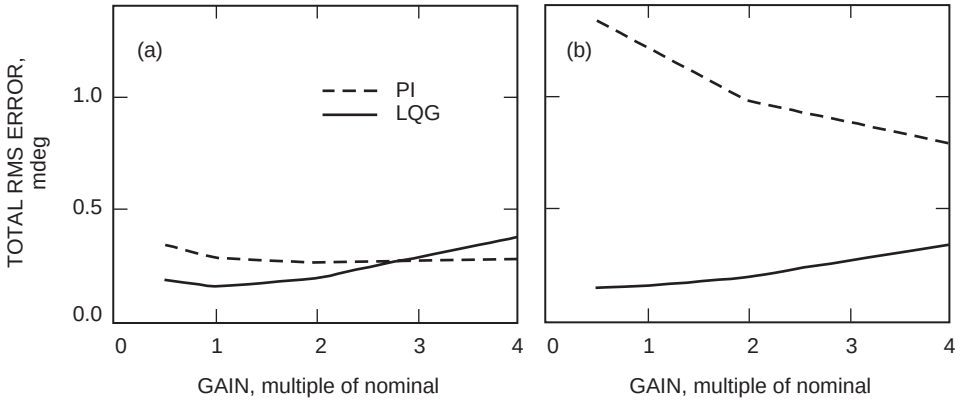

Fig. 15. Monopulse system error under total disturbances: (a) azimuth and (b) elevation.

The block diagram of the monopulse pointing-error detector is shown in Fig. 16(b). This nonlinear device transforms the azimuth and elevation pointing error into the elevation and cross-elevation pointing error. It consists of the converter of azimuth and elevation angles into θ and ϕ parameters, nonlinear functions $g(\theta, \phi)$ and $h(\theta, \phi)$, and other nonlinear functions [such as $\sqrt{(\cdot)}, \sin(\cdot)$, and $\cos(\cdot)$]. The detector functions $g(\theta, \phi)$ and $h(\theta, \phi)$ are shown in Figs. 17(a) and 17 (b) for the 15-dB signal-to-noise ratio (SNR). They depend on the size of the null depth. Additionally, the detector model consists of disturbances

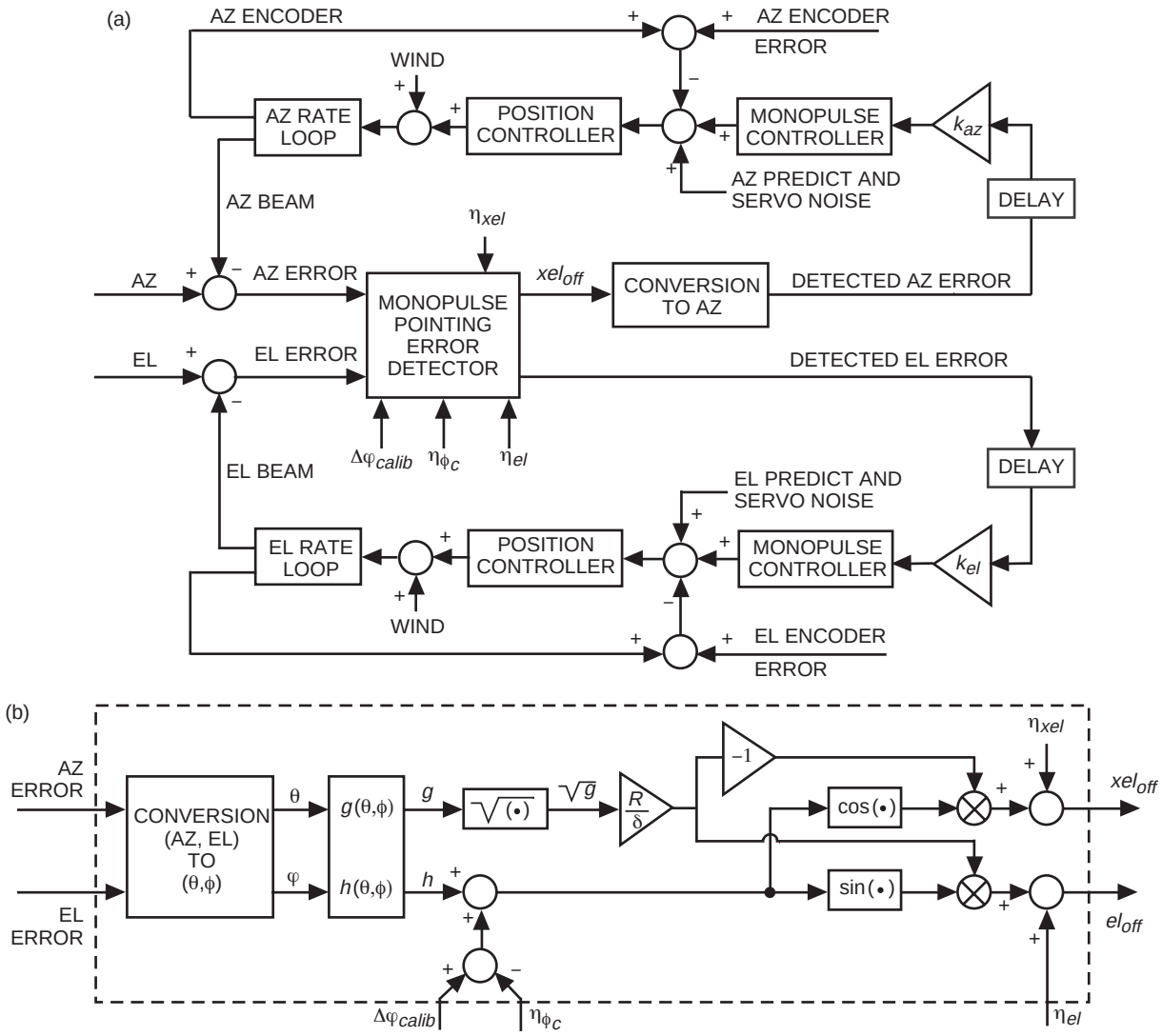

Fig. 16. Block diagrams of (a) the nonlinear monopulse control model and (b) the monopulse pointing model detector.

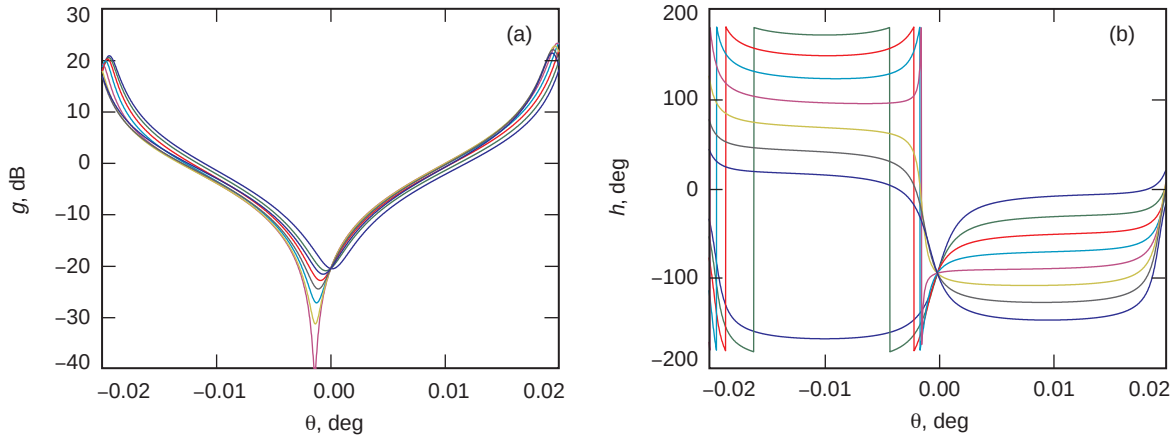

Fig. 17. The detector functions for an SNR of 15: (a) *g* and (b) *h*.

and noises that represent its imperfections or environmental interactions—namely, the boresight shift, $\Delta\phi_{calib}$; the BVR noise, η_{el} and η_{xel}; and the receiver demodulation noise, η_{ϕ_c}. The detector couples azimuth and elevation error; therefore, the errors cannot be determined separately. In consequence, the nonlinear control system model combines azimuth and elevation loops together, as in Fig. 16(a). This model includes, besides the detector, converters from the cross-elevation, elevation coordinates to azimuth, elevation coordinates, time delays (of 0.1 s), variable loop gains k_{az} and k_{el}, monopulse controllers, position controller (LQG), and azimuth and elevation rate loop models. This closed-loop system is subject to wind disturbances, servo noises, and encoder errors, and is driven by the azimuth and elevation commands.

Extensive simulations of the nonlinear closed-loop system that depend on the above-listed parameters have been performed. The results are summarized in Fig. 18, showing the elevation and cross-elevation errors for the 5-mdeg step offset in elevation and cross-elevation. The target of 5 mdeg in elevation and 5 mdeg in cross-elevation is acquired. The error depends on the SNR. For a high SNR of 40 dB, the radius of the circling of the destination point of (5, 5) mdeg is small, about 0.5 mdeg. For an SNR of 27 dB, it increases to about 1 mdeg (the extra "ears" are due to azimuth encoder imperfections); for an SNR of 20 dB, it is about 2 mdeg; and for an SNR of 12 dB, it is about 5 mdeg.

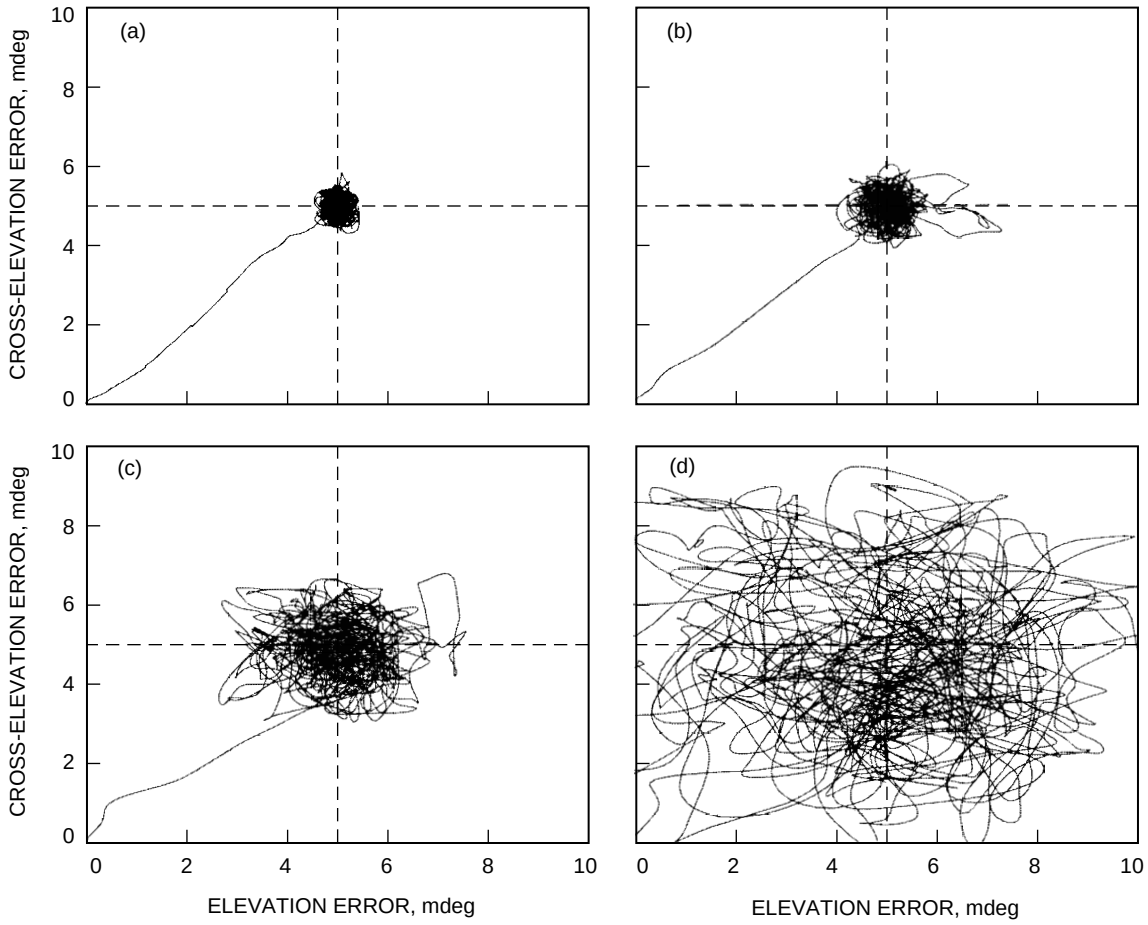

Fig. 18. Elevation and cross-elevation errors for the 5-mdeg step offset in elevation and cross-elevation, and for an SNR of (a) 40 dB, (b) 27 dB, (c) 20 dB, and (d) 12 dB.

The radial error $\theta(t)$ often is used as an indicator of the system performance. It is defined as

$$\theta(t) = \sqrt{\varepsilon_{el}^2 + \varepsilon_{xel}^2}$$

where ε_{el} and ε_{xel} are the elevation and cross-elevation errors, respectively. The mean radial error (MRE) consequently is a mean of $\theta(t)$:

$$MRE = E(\theta(t))$$

The plots of $\theta(t)$ for different SNR ratios are shown in Figs. 19. In this figure, the histograms of the error are presented. The MRE diagram versus SNR is given in Fig. 20.

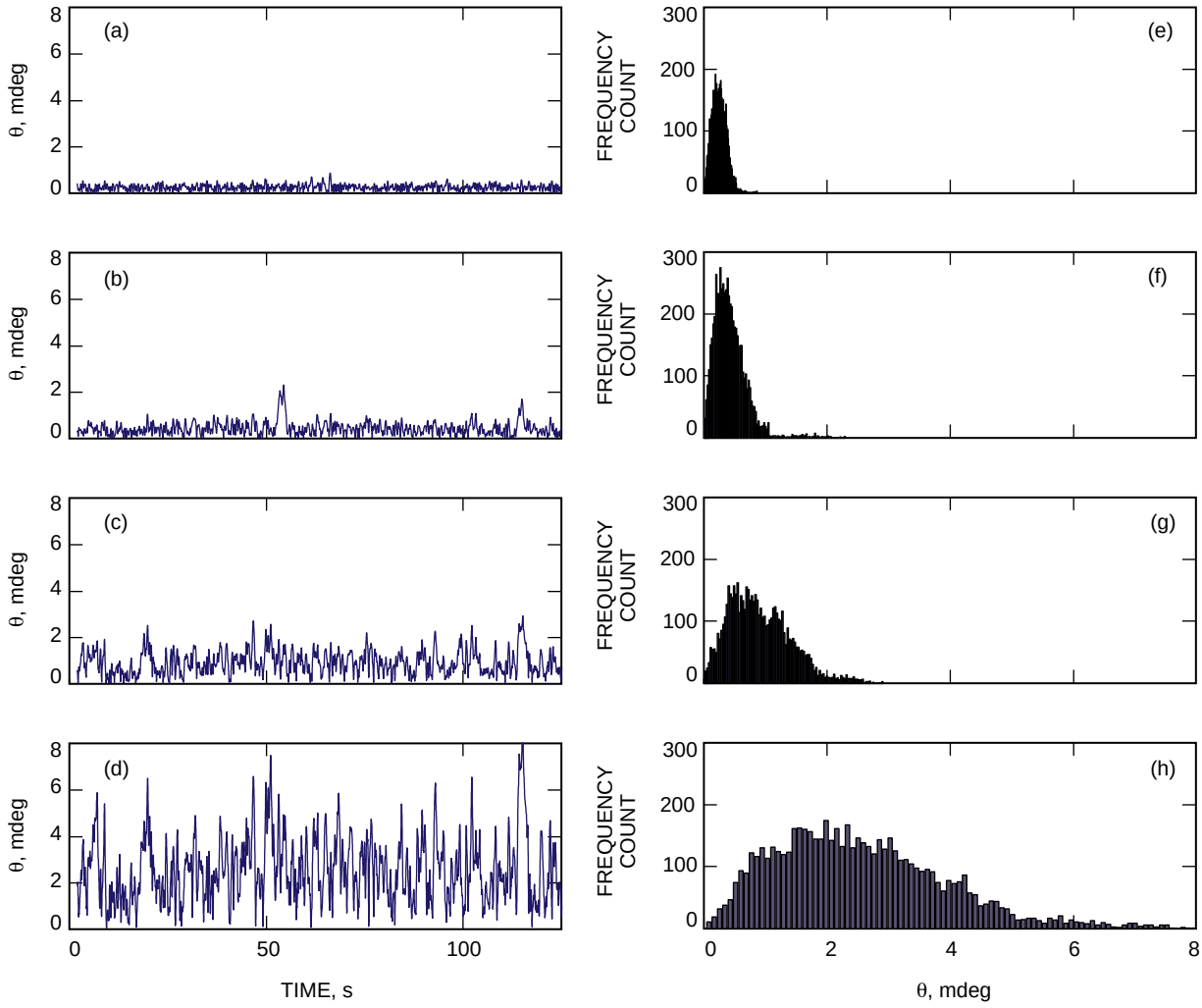

Fig. 19. The plots of radial error, θ(*t*), for different SNR ratios: (a) 40 dB, (b) 27 dB, (c) 20 dB, and (d) 12 dB, and its frequency counts: (e) 40 dB, (f) 27 dB, (g) 20 dB, and (h) 12 dB.

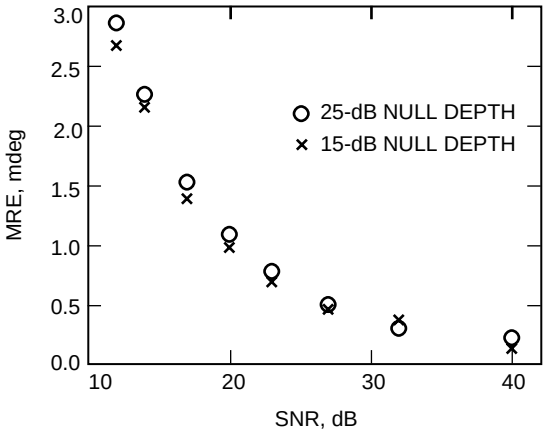

Fig. 20. The MRE versus SNR.

V. Conclusions

The monopulse controller was designed and analyzed, and its performance was verified through extensive simulations. It has been shown that the 1.54-mdeg-error pointing requirement will be met if the antenna is equipped with the high-gain LQG control algorithm.

Acknowledgments

We thank William Hurd for helpful discussions and Paula Brown and Luisio Prata (USC) for the models of the ideal and degraded monopulse feed and antenna patterns.

References

[1] W. Gawronski, C. Racho, and J. Mellstrom, "Application of the LQG and Feedforward Controllers for the DSN Antennas," *IEEE Trans. on Control Systems Technology*, vol. 3, pp. 417–421, 1995.

[2] W. Gawronski and J. A. Mellstrom, "Control and Dynamics of the Deep Space Network Antennas," chapter in *Control and Dynamic Systems*, ed. C. T. Leondes, vol. 63, San Diego: Academic Press, 1994.

[3] G. Biernson, *Optimal Radar Tracking Systems*, New York: Wiley, 1990.

[4] W. Gawronski, "Wind Gust Models Derived From Field Data," *The Telecommunications and Data Acquisition Progress Report 42-123, July–September 1995*, Jet Propulsion Laboratory, Pasadena, California, pp. 30–36, November 15, 1995. http://tmo.jpl.nasa.gov/progress_report/42-123/123G.pdf